Approaches to Embryonic Neurodevelopment: From Neural Cell to Neural Tube Formation through Mathematical Models

Ali H. Rafati

ali.h.rafati@clin.au.dk

Aarhus University

Sâmia Joca

Aarhus University

Regina T. Vontell

University of Miami Miller School of Medicine

Gregers Wegener

Aarhus University

Maryam Ardalan

University of Gothenburg

Article

Keywords: Embryonic Period, Mathematical Equations, Neurodevelopment, Natural Transformation, Topological Spaces

Posted Date: January 25th, 2024

DOI: https://doi.org/10.21203/rs.3.rs-3873839/v1

Additional Declarations: No competing interests reported.

Approaches to Embryonic Neurodevelopment: From Neural Cell to Neural Tube Formation through Mathematical Models

Ali H. Rafati[1*], Sâmia Joca[1,3,4], Regina T. Vontell[5], Gregers Wegener[1], Maryam Ardalan[1, 2]

1) *Translational Neuropsychiatry Unit, Department of Clinical Medicine, Aarhus University, Aarhus, Denmark*
2) *Institute of Neuroscience and Physiology, Centre for Perinatal Medicine and Health, Sahlgrenska Academy, University of Gothenburg, Gothenburg, Sweden*
3) *Center of Functionally Integrative Neuroscience-SKS, Department of Clinical Medicine, Aarhus University, Aarhus, Denmark*
4) *Department of Biomedicine - Forskning og uddannelse, Vest, Aarhus University, Aarhus, Denmark*
5) *Department of Neurology, University of Miami Miller School of Medicine, Brain Endowment Bank, Miami, USA*

***Corresponding author**

Translational Neuropsychiatry Unit, Department of Clinical Medicine, Palle Juul-Jensens Boulevard 11, 8200 Aarhus N, Denmark,

ali.h.rafati@clin.au.dk

Running title: Embryonic Neurodevelopment through Mathematical Models

Abstract

The human central nervous system (CNS) undergoes development from early embryonic stages to well beyond birth, with various neurological and neuropsychiatric diseases originating from prenatal events. Mathematical models offer a direct avenue for understanding these neurodevelopmental processes, particularly during the embryonic period. However, approaching and initiating such modeling presents challenges, including the formulation of appropriate equations that capture the dynamics of neurodevelopment.Therefore, this study aimed to comprehensively address the mathematical challenges by exploring different approaches. The approaches were divided into three embryonical categories: *cell division, neural tube growth and neural plate growth.* We concluded that *the neural plate growth approach provides a suitable platform for simulation of brain formation/neurodevelopment compared to cell division and* neural tube growth. We devised a novel equation and designed algorithms that include geometrical and topological algorithms that could fit most of the essential elements of the neurodevelopmental process during the embryonic period.

Keywords: Embryonic Period, Mathematical Equations, Neurodevelopment, Natural Transformation, Topological Spaces

Introduction

Human brain development is a process in which so-called neurodevelopment occurs according to a specific time frame. It starts in the third gestational week with differentiation of the neural progenitor cells, lasting until late adolescence. Different types of cascades lead to neurodevelopment, from genetic mutation to environmental factors [1,2]. However, there is no reliable parameter for early detection or prediction of alteration in CNS development. Models that use mathematical concepts offer insight into the neurodevelopmental process and attempt to shed light on the underlying mechanisms of developmental processes in mathematical equations. In mathematical modelling of the neurodevelopmental processes, one of the biggest challenges is how to "approach", meaning where to begin, and how to look at this entity for inspiration for computation/neural networks, but more importantly, to understand the underlying mechanisms that drive neurodevelopment during embryonic development [2,3]. Our previous study addressed these questions at a preliminary level [4]. Eventually, we devised an equation that theoretically showed neuronal clustering in the cortex [5] by using the cellular characteristics, since such descriptions are limited [4], this study addresses these fundamental questions using more complex equations and algorithms. We explore the possibilities and pitfalls to understand how neurodevelopmental processes during embryogenesis can be analyzed mathematically. An embryonic neurodevelopmental dynamic modelling of this specific perspective is presented time in this study. Recent research [3] provided a mathematical model that frames how the brain network grows over the developmental period based on an equation that predicts the wiring between different brain regions. Using this framework, they showed diversity in neurodevelopment, a function of the wiring equation in terms of connectivity. However, the details of cellular components underlying neurodevelopment remain to be discovered and expressed [3]. Accordingly, our study aimed to clarify different types of mathematical modelling for neurodevelopmental processes based on 3 different approaches: Approach-1: Cell Division to Neurodevelopment; Approach-2: Neural Tube development; Approach-3: Neural Plate Development.

Results

1.Different Types of Approaches to Neurodevelopment: Mathematical Modelling and Their Pitfalls

To make the data more comprehensible and be able to model neurodevelopement meaningfully according to what happens naturally, we divided neurodevelopment into following steps: 1´. Cell division, 2´. Neural tube development, 3´. Neural plate development to become comparable in mathematical modelling (**Figure 1**). The bottom line is to indicate how to match these models with biology, where our understanding must include the following mathematical entities: the first one would be holomorphic functions that indicate continuity and are defined by complex-valued function; and also, to implicate

group homomorphism, which is expressed by h: G→H. The group homomorphism implies that it can generate a preserved map while transforming from one structure to another one, this process fits well with biology, such as tissue growth and development.

2.A. Approach-1: From Cell Division to Neurodevelopment

Cell cell division and polarity have been shown as deterministic in cells in relation to orientation and organization, so if we consider cell division patterns and polarization as illustrated in **Figure 2.A**, we must be able to provide a mathematical model that fits all neurodevelopment steps. Still, it did not sound plausible based on the cell division and cellular polarization. We decided to use the cell membrane that is composed of complex filaments (**Figure 2.B**). which is called the "cellular cortex" [6] for simulating the cell division. The "cellular cortex" is an actin network connecting to the cell membrane containing myosin-2 motors. The function of the cellular cortex is to determine the cell shape, polarization, and it is actively involved in cell division, migration and tissue morphogenesis [6,7].

We applied the rational Bézier curves using the weighted Bernstein-form, the W stands for the weight that receives the complex values, and the Pi stands for the points and $0 \leq t \leq 1$, which is shown in Equation.1. We assumed that the generated convex body (**Figure 3**) by these sequential Bézier curves around the centre in 3D space simulates a cell that is dividing, so for simplicity, we used the curves to continue until to generate a brain tissue like the one in **Figure 2.A**. Equivalently, it is called "Winding Number" which is defined by the number of times that a continuous curve travels around the certain point/points [8] (**Figure 3**). Alternatively, one could think of the "kissing number" [9] that is packing of spheres in a specific space, like in **Figure 1. A**.

$$(1)\quad B(t) = \frac{\sum_{i=0}^{n} \mathrm{bi}, n(t)\,\mathrm{PiWi}}{\sum_{i=0}^{n} \mathrm{bi}, n\,(t)\mathrm{Wi}} \qquad or \qquad B(t) = \frac{\sum_{i=0}^{n} \binom{n}{i} t^i\,((1-t)^{n-i})\mathrm{PiWi}}{\sum_{i=0}^{n} \binom{n}{i} t^i\,((1-t)^{n-i})\mathrm{Wi}}$$

However, it implies that we are restricted in modelling the biological structures mathematically since approximation to the biological structure by applying mathematical models is rather sophisticated. Consequently, the pitfalls and possibilities are remarkable for this approach, "From Cell Division to Neurodevelopment". Therefore, as this approach did not help to continue modelling for the rest of the brain development, we used another equation using a different mathematical method instead. It is quite complex to generate a simulated tissue and demonstrate the natural process of neurodevelopment.

2.B. Approach-2: From Neural Tube Formation to Neurodevelopment

In this approach, we defined a neural tube development similar to the Möbius plane [10]. Here, we designed $B:=\{C, S, S'\}$ in which C indicates the curve like Equation.2 and S & S´ indicates two spaces (equivalent to two brain hemispheres and symmetry in CNS) that cross at crossing points on curve C as shown in **Figure 4.A**.

(2) $B:=\{C,S,S'\},\ B(t)=\big(C(t),S(t),S'(t)\big)$ in R^2

In fact, equation "B (t)" is helpful in guiding it's the appropriate parametrization as shown in equation.3 that is demonstrated in **Figure 4.B**. Thus, this equation reflects the symmetry that we observe in the CNS.

(3) $L=\zeta(\mathrm{e}^{\pi\, x\, y\, 1\mathrm{i}})$, $-20\le x\le 20, -1\le y\le 1$, i is an imaginary value.

We further used equation 3 to generate a single-cell neuron model. Furthermore, we developed Equations 4 and 5 by applying "*Lambert W function*" and the Riemann–Siegel theta function [11], a gamma function that has also been included in both Equations3 and 4. Using these two equations we were able to demonstrate a neuron schematically (**Figure 5.A to C**). A to C looks like a neuron schematically. This single neuron can be integrated into the mathematical model of CNS structure similar to the model in Equation 3; however it shows limited options when we try mathematically design the model by inserting the single neuron as a unit building blocks for model "B(t)" shown in **Figure 4**. However, it shows limited options when we try to mathematically design the model by inserting the single neuron as a unit building block for model "B(t)" shown in **Figure 4.A**. However, despite providing these equations for single neuron and CNS models at this step via this specific approach, it seems impossible to give a *general equation* covering all neurodevelopment stages. Accordingly, this is the downside of this model since we could not clearly define how cells could be built up through this model and via this approach in light of the complexity of the CNS and especially the trajectories. We decided to develop an equation that could deal with most of the issues of cell build-up and trajectories, if not.

(4) $t=\dfrac{2\pi\left(n+\frac{1}{8}\right)}{\mathrm{W}_0\left(\mathrm{e}^{-n-\frac{1}{8}}\right)},\ \theta(t)=-\dfrac{\ln(\pi\, t)}{2}-\dfrac{\ln\left(\Gamma\left(\frac{1}{4}+\frac{t\, y\, 1\mathrm{i}}{4}\right)-\ln\left(\Gamma\left(\frac{1}{4}-\frac{t\, y\, 1\mathrm{i}}{4}\right)\right)\right)1\mathrm{i}}{2}$, If $T=\theta(t)$, then …

$F=\mathrm{e}^{\pi\, T\, x\, y\, 1\mathrm{i}}$, $-20\le x\le 20,\ 0.1\le y\le 1,$ If $T=\theta(t)$ and $-2\le n\le 6$.

(5) $\theta(t)=-\dfrac{\ln(\pi\, t)}{2}-\dfrac{\ln\left(\Gamma\left(\frac{1}{4}+\frac{t\, y\, 1\mathrm{i}}{4}\right)-\ln\left(\Gamma\left(\frac{1}{4}-\frac{t\, y\, 1\mathrm{i}}{4}\right)\right)\right)1\mathrm{i}}{2}$, If $T=\theta(t)$, then $F=\mathrm{e}^{\pi\, T\, x\, y\, 1\mathrm{i}}$, …

$-20\le x\le 20$, $0.1\le y\le 1$, and t is imaginary numbers.

2.C. Approach-3: From Neural Plate Formation to Neurodevelopment

This approach requires exploring the factors determining the ultimate 3D structure of a tissue and an organ such as the brain, heart, etc. The relevant mathematical theory, called "Representation Theory" (12), explores how the linear transformation is applied on vector spaces and geometrical objects and studies topological methods. We postulated that to generate a 3D structure of CNS geometrically, there should be a 3D map along the z-axis to guide us on how to grow the tissue in a stepwise manner according to a certain numerical map (**Figure 7.2**). Therefore, we need to design the bijective map (**Figure 6.D**) similar with Cayley Groups table [12] such that F: $G_1 \rightarrow G_2$, however it differs in our model based on how the changes occur on the table. As there is an automorphism in our model such that the tissue in the (x-y) plane regenerate themselves, the mapping and changes on the (x-y) plane are transferred in the z-axis direction according to **Figure 7.2.A & B**. This process is equivalent to neuronal tissue growth. To determine the amount of cell growth and development, we need a numerical map that is geometrically isomorphic [13] in the z-axis from one layer of tissue to another. As a result, we provide some examples of a (x-y) plane and a numerical map demonstrated in **Figure 7.1.A & B**, respectively. **Figure 7.1.B** shows that the numerical map could be a Pascal triangle. Thus, the z-axis must be assigned with a numerical map for each tissue/organ individually, which might be considered specific and constant to that tissue/organ. Similarly, the analogous numerical map to the Pascal triangle is the well-known Hermite polynomials [14], $H_n(x) = (-1)^n e^{x^2} \frac{d^n}{dx^n} e^{-x^2}$ that yields the following polynomials of degree n: $\mathrm{H}_0(\mathrm{x})=1$; $\mathrm{H}_1(\mathrm{x})= 2\,\mathrm{x}$; $\mathrm{H}_2(\mathrm{x})= 4\,\mathrm{x}^2 - 2$; $\mathrm{H}_3(\mathrm{x})= 8\,\mathrm{x}^3 - 12\,\mathrm{x}$.

Therefore, before explaining our equation for this approach, we provide some relevant mathematical equations that could be equivalent to our equation, summarized in **Figure 7.3**. They must provide information about the curves, surface, or transformation from one shape to another. However, to meet our requirements for designing a tissue/organ mathematically which are in form of schematic illustrations and are collectively summarized in **Figure 6**. The first function of this kind is called "*shape operator*" [15-17], which is defined by: $S_p(v)=-\nabla_v N$. The *p* stands for a point on surface *M*, the normal vector at point *p* is *N,* and *v* is a tangent vector on *M* at *p.* Then, any change in the surface area around the point *p* can be estimated. It has been demonstrated in **Figure 6.A**. It provides information about the shape of curves in terms of their normal vector on the curves and the direction of change in curvatures. Another definition related to the shape operator uses the principal curvatures and principal directions, equivalently called "*eigenvalues and eigenvectors"*. Thus, the parameters define the shape change of a geometrical object (**Figure 6.A**). Moreover, the relevance to shape transformation could be obtained by applying the "*linear transformation"* [18]. Generally, the "*linear transformation",* which is also called "*linear mapping* or *linear operator",* is defined as follows: if XY considered vector space, then there would exist x and y as vectors

that belong to X and Y, respectively and y is the image of x by *F* function, expressed by y=F(x), (**Figure 6.B**). Another relevant entity is dynamical systems related to differential geometry in which the configuration of manifolds is studied. Dynamical systems could be categorized into nonlinear and linear [19]. As an example, the "*Koopman operator"* [20] has been defined as an infinite-dimensional operator that applies in nonlinear dynamic systems. The other example is the orthogonal polynomial indicated by orthogonal functions in 3D space. Another related entity applicable in the geometrical application for dynamic systems is the "*parabolic cylinder coordinate"* [21]. That can be expressed based on hypergeometric function. As the cylinders organize and orient concerning manifolds, this mathematical analogy can be applied to organizing tissue/organ geometrically (**Figure 6.C**). The parabolic cylinder function is denoted by $D_v(z) = 2^{(v/2)}e^{(-z^2/4)}U(-1/2\, v, 1/2, 1/2\, z^2))$ [22]. In the next step, two essential steps of our main equation are presented in a simplified form by mathematical equations explained in **Figure 7**. At this step, we provide more information about our equation by defining the "*linear/vector subspace"*. If we assign the "*linear/vector subspace"* as A in a finite field [23] of B, which is R^2, then we can obtain the linear equations related to the subspace by setting the points (x, y) in R^2. If the fixed vectors are added into a vector/linear subspace, it could be d "*affine space"* [24]. Thus, the affine subspace is denoted by having a subspace B that belongs to affine space A such that by setting the points $b \in B$ and containing vectors $\vec{C}$ that make the linear subspace B. Hence, for every point such that $b_n \in B$, there is a vector called $\vec{C}$ that projects the point b_n by function F. In general, the subspaces belongs to modular lattice (Dedekind lattices) which has been defined elsewhere [25]. Further, we generated the linear/vector subspace in relation to polynomial expansion through "*Pascal's triangle"* [26] as a binomial coefficient (**Figure 7.2.C**). The summarized explanation of the equation is demonstrated in **Figure 7.2**. It requires explaining why we use "*Pascal's triangle"* and the related polynomial expansion. Each 3D tissue/organ formation must be assigned a set of magic numbers that guides how much the tissue/organ must develop numerically in the z-axis to take the final 3D shape. This set of magic numbers could differ based on the tissue/organ of the animal/human. Thus, we proposed the equation in **Figure 7.3**. It explains the relation between the "*linear/vector subspace"* and "*Pascal's triangle",* which is assigned as a set of magic numbers for neuronal tissue formation. Nevertheless, another study is required to explore how these individualized magic numbers are assigned to different tissues and organs. In the next step, we defined our main equation that is obtained accordingly, as shown below in Equation. 6. We first defined the elements and main contributors to the Equation. 6, including the formulated cellular properties in conjunction with the *Riemann–Siegel theta* function shown in Equation.5. The similar operations regarding our introduced Equation. 6 have been demonstrated by discussing the "*Weierstrass Sigma-Functio"* and "*elliptic function"* and "*partial differential equation"* (PDE) [27,28]. The following steps demonstrated how the

partial differential equation (PDE) is applied to generate the Equation. 6 by using the $\mathbf{G_n}$, $\boldsymbol{\theta}(\boldsymbol{G_n}, \boldsymbol{t})$ and $\boldsymbol{E}(\boldsymbol{G_n}, \boldsymbol{\theta_n})$, sequentially. It implies how the cellular properties acts through the fowling mentioned equations to affect the cell cycle and growth in the schematic illustration.

- $\mathbf{G_n}= [\mathrm{G_1(X)}, \mathrm{G_2(Y)}, \mathrm{G_3(Z)}]$, $G'= N$, $x_i = [X, Y, Z]$ and $x_i \in R$
  - $\boldsymbol{N}= \nabla \times F = \begin{vmatrix} \hat{\imath} & \hat{J} & \hat{k} \\ \frac{\partial}{\partial X} & \frac{\partial}{\partial Y} & \frac{\partial}{\partial Z} \\ G_1(X) & G_2(Y) & G_3(Z) \end{vmatrix}$, *the cellular properties*
  - $\boldsymbol{N} = \left[\left(\frac{\partial G_Z}{\partial Y} - \frac{\partial G_Y}{\partial Z}\right) i + \left(\frac{\partial G_X}{\partial Z} - \frac{\partial G_Z}{\partial X}\right) j + \left(\frac{\partial G_Y}{\partial X} - \frac{\partial G_X}{\partial Y}\right) K\right] \approx \begin{bmatrix} \left(\frac{\partial G_Z}{\partial Y} - \frac{\partial G_Y}{\partial Z}\right) i \\ \left(\frac{\partial G_X}{\partial Z} - \frac{\partial G_Z}{\partial X}\right) j \\ \left(\frac{\partial G_Y}{\partial X} - \frac{\partial G_X}{\partial Y}\right) K \end{bmatrix}$
  - $\boldsymbol{\theta}(\boldsymbol{G_n}, \boldsymbol{t}) = \frac{-\ln(\pi\, t)}{2} - \frac{\ln\left(\Gamma\left(\frac{1}{4} + \frac{t\, G_n\, 1i}{4}\right) - \ln\left(\Gamma\left(\frac{1}{4} - \frac{t\, G_n\, 1i}{4}\right)\right)\right) 1i}{2}$, $n \in \{1,2,3\}$
  - $\boldsymbol{E}(\boldsymbol{G_n}, \boldsymbol{\theta_n}) = (e^{G(X)\pi\,\theta_1})\hat{\boldsymbol{e}}_{\boldsymbol{1}} + (e^{G(Y)\pi\theta_2})\hat{\boldsymbol{e}}_{\boldsymbol{2}} + (e^{G(Z)\,\pi\,\theta_3})\hat{\boldsymbol{e}}_{\boldsymbol{3}}$
  - $\boldsymbol{Ah}(\boldsymbol{x}) = H(x, h(x), \ldots, \partial^m_{x1\ldots xn} h(x))$, differentiable function of *F,* then the 2nd order partial differential equation (PDE) is defined as $\mathbf{D}(\boldsymbol{x}) = \sum_{1\le j\le k\le N} C_{j,k}(x)\partial^2_{j,k}h(x) + \sum_1^N C_i(x)\partial_i h(x)$ [29,30].
  - $n \in \{1,2,3\}$, $A = C = D = E = 1$;
  - $B_i = \left(\frac{\partial G_Z}{\partial Y} - \frac{\partial G_Y}{\partial Z}\right) i$, $B_j = \left(\frac{\partial G_Z}{\partial Y} - \frac{\partial G_Y}{\partial Z}\right) j$, $B_K = \left(\frac{\partial G_Y}{\partial X} - \frac{\partial G_X}{\partial Y}\right) K$

(6) $$\boldsymbol{D}_{\hat{\boldsymbol{e}}_{\boldsymbol{n}}} = A\frac{\partial^2 E_{\hat{\boldsymbol{e}}_{\boldsymbol{n}}}}{\partial G_n^2} + B_n\frac{\partial^2 E_{\hat{\boldsymbol{e}}_{\boldsymbol{n}}}}{\partial G_n \theta_n} + C\frac{\partial^2 E_{\hat{\boldsymbol{e}}_{\boldsymbol{n}}}}{\partial \theta_n^2} + D\frac{\partial E_{\hat{\boldsymbol{e}}_{\boldsymbol{n}}}}{\partial G_n} + E\frac{\partial E_{\hat{\boldsymbol{e}}_{\boldsymbol{n}}}}{\partial \theta_n}$$

We showed the black curves that stretch vertically; they are the "*Bezier curve*" that their vectors of "M" generate them, and the curve is controllable by "W", so $M_{t+dt} = M_t + M_{dt}$, the "t" is obtained by the "*Runge-Kutta"* method [31,32]. The "*Runge-Kutta"* method is " $K_1 = hf(x_n + y_n)$; $K_2 = hf(x_n + (1/2)h,\ y_n + (1/2)k_1)$; $y_{n+1} = y_n + K_2 + 0\ (h^3)$", which is number solution method to our equation. 6 and generates input $D_{\hat{e}n}$=$\{D_{\hat{e}_1}, D_{\hat{e}_2}, D_{\hat{e}_3}\}$ for W=$\{W_{\hat{e}_1}, W_{\hat{e}_2}, W_{\hat{e}_3}\}$ in three axes. Therefore, the "*Bezier curves"* are generated in three axes like a 3D object which is not shown here and only one direction is shown in Figure.7.3. In addition, the singular value decomposition (SVD) is denoted by $M = U\sum V^*$ in which U and V unitary matrices and Σ is diagonal matrix. In the next step, we explained the "B(t)" in **Figure 7.3** is a so-called *binomial formula* that generates the *Pascals triangle;* meanwhile, it uses $t_{\mathbf{1}:\boldsymbol{n}}$ to assign the equation of t_3 and t_5 for the developing cells (linear subspace), as an example, is shown in **Figure 7.3**. When, these curvilinear lines are generated by *a* binomial formula, they determine the whole shape of the developing tissue structure in that section. If we consider t_3 *and* t_5, this expression $\mathbf{10}\,\boldsymbol{x^3y^2}$ from t_5 could be removed as this third part is equivalent to the singularity point in **Figure 7.2. B**. Regarding the singularity, the Maclaurin series can be applied based on the singularity, non-isolated set such as a boundary with no analytic function around it [33], but in case of isolated

singularity point can be explored by Laurent expansion, $f(z) = \sum_{-\infty}^{\infty} a_n (z-c)^n$, a_n is the coefficient and also in case of meromorphic function (complex function), can be used and investigated for singularities. Next in the below, "c" shows the t_5 transforms to $t_{5,2}$ Then, the new plot is generated from the new equation to generate a different plot depending on the equations. We think this also happens in biology when the type of the cells varies along a certain cell line, so in this case, they can be considered as singularity point/points. That point is removed from the equation whenever the singularity *point/points* are not replaceable by Laurent expansion.

a) $B = \sum_{k=0}^{n} \binom{n}{k} x^{n-k} y^k,\ if\ k \le n\ \&\ t_{\mathbf{1:n}}$

b) $t_3 = x^3 + 3x^2y + 3xy^2 + y^3$;

c) $t_5 = x^5 + 5x^4y + \mathbf{10}\,\boldsymbol{x^3y^2} + 10x^2y^3 + 5xy^3 + y^5 \rightarrow t_{5,2} = x^5 + 5x^4y + 10x^2y^3 + 5xy^3 + y^5$

d) ⟨1 2 **3*singularity*** 4 5 6⟩ It is the third cell on the orange line that is singularity, so we remove the 3rd on the equation.

Briefly, the whole process is summarized in **Figure 7.3.**

Alternatively, we may model the neuronal cell morphology and development in connection with electrical activity and chemical factors and explore how it naturally would change and evolve. Therefore, regarding the topology, we can apply the functors and natural transformation [34,35] from category theory. The functions are defined by the morphism and objects demonstrated in the **Figure 8.A**. Each category has its own certain structure, and the functions consist of the elements called objects that belong to the certain category. The morphisms are canonical maps, for example**, *f***: M1 ⟶ M2, the M1 and M2 are denoted as objects, and ***f*** is the morphism that maps from M1 to M2. The functors of our diagram are defined as a parallel pair E and C, from categories A and B such that $E, C: A \Rightarrow B$.

In **Figure 8.A**, the first category is called "*A*" that contains f: M1 ⟶ M2, which implies that M1 and M2 are objects, and M2 is mapped by morphism "***f"***. The M1 and M2 are representative of manifolds of a certain type of neuronal cell that, in the next step at category "*B*", is transformed into E(M1) and C(M1), representing electrical activity which is Functor "E" and chemical factors which is Functor "C", respectively. They are involved in influencing the cell morphology (M: manifolds) and consequent functional changes. The effect of *natural transformation* is defined by Φ(M1) and Φ(M2). Thus, the E(M1) and E(M2) are transformed into the C(M1) and C(M2), which is a function of the *natural transformation,* which is defined by changing the functions from E to C. Thus, the relations of *natural transformation* are denoted as Φ= {Φ(M1): E(M2) ⟶C(M2) | M2 ∈ B}. Then it is namely "*commutes"* as follows: Cf o Φ(M1) = Φ(M2) o Ef.

We further explained how to define topological spaces, including neuronal cells embedded in a growing compact tissue, mathematically. First, this tissue (here we mean the neuronal tissue) is considered a finite topological space 'S', which consists of two elements (X, τ_m) that X is the non-countable part, such as the extra-cellular matrix and τ_m is the differentiable *manifold* that is the countable part like the neuronal cells (NC) such that (X $\cap$ τ_m)$\neq \emptyset$. Therefore, it satisfies the *Lindelöf space* and is *Hausdorff,* where all topological manifolds belong [36-38]. Thus, there exist subspaces such that U_1, $U_n \subset S$, ($U_1 \cup U_n$) $\subset$ S and ($U_1 \cap U_n$) ϵ S. The τ_m can be defined as differentiable manifolds that are countable and compact. The relation between the NC is as follows if $NC_1, \dots, NC_i, NC_n$ then $NC_1 \cap NC_i \cap NC_n \neq \emptyset$. In addition, since the tissue grows continuously and changes in shape from the original tissue structure and morphology, it can be considered as a *quotient space* [39] such that G: $(X, \tau_m) \rightarrow (Y, \tau_n)$. Further, the quotient space could be regarded as a *Banach subspace* where referred to as vector space which is by definition *a Hilbert space* [40]. As we defined the neuronal cells as analogous to a differentiable manifold that is indicated by every point $p_{\{x,y,z\}}$ such that $R^n = \{(x_1, x_i, x_n): x_i \in R \; for \; i = 1, n\}$ and $\{x, y, z\} \in R^n$ on the differentiable manifold "*M",* which is denoted by $d\left(NC_{\boldsymbol{p}_{\{x,y,z\}}}\right) = \frac{\partial f(M)}{\partial x_i}$ equation. Next, it is essential to mention the other factors that exist in association with the cells and regulate independently the fate of cellular development. They are collectively called thermodynamic laws [41,42]. The Gibbs free energy that combines the enthalpy and entropy and thus is related to the thermodynamic laws has a deterministic role if a chemical reaction process can continue in a certain direction [43]. The fundamental equations for Gibbs energy are denoted by $G = U + pV - TS$, it consists of U the internal energy, P the pressure, V the volume, T the temperature and S the entropy. The differential for Gibbs is defined by $dG = -SdT + Vdp + \sum_{i=1}^{N} \mu_i \, dn_i$ in which n_i the amount of particles and μ_i the chemical potential of the particle and N, the number of particles [41]. This chemical factor in the form of differential for Gibbs that is described here is assumed to be the contributing factor that leads to the change in the manifolds that are presented in **Figure 8** as Functor C: Cf(M1)→Cf(M2). Further, the electrical activity (E) of the cells is regarded as another independent factor that contributes to the morphological change of the cells (assuming the change in the manifolds shown in **Figure 8** as Functor E: Ef(M1)→Ef(M2)) and leads to cellular growth. The equation is called the Van der Pol equation [4] and is applied to generate the vector field in two-phase, which is $\dot{x}_2 = -x_1 - m(x_1^2 - 1)x_2$, m = 0.1 and m = 1, E= $\dot{x}_2$.

Finally, we have to define the calculation of **Figure 8.D**, which is, in summary, the flow of the vector field that affects and interacts with every point. $p_{\{x,y,z\}}$ of the differentiable manifold, $d\left(NC_{\boldsymbol{p}_{\{x,y,z\}}}\right) = \frac{\partial f(M)}{\partial x_i}$. It is reminded that there is a unified approach that deals with manifolds with higher dimensions in the field of geometry and topology called differential forms, explained by Cartan [44]. It is

applicable when we express the effect of the vector field on the differentiable manifolds. In our model, there are two vector fields E and C, which are denoted by $\alpha(E)_k$ and $\beta(C)_l$ on point p such that $p \in d\left(NC_{\boldsymbol{p}_{\{x,y,z\}}}\right)$. There exists $(X_{S(1)}, X_{S(i)\dots}, X_{S(k)}) \in f(M)_p$. Thus, their *wedge product* is denoted by the following equation $(\alpha \wedge \beta)(X_{S(1)}, X_{S(i)\dots}, X_{S(k)}) = \frac{1}{K!l!}\sum_{S\in S(k+1)} \text{sign(S)}\, \alpha(X_{S(1)}, X_{S(i)\dots}, X_{S(k)}) \dots \beta(X_{S(k+1)}, X_{S(i)\dots}, X_{S(k+1)})$. The differential k-form can be defined in general form with $\alpha_{i1} \dots \alpha_{ik} = \alpha\left(\frac{\partial}{\partial x^{i1}}, \dots, \frac{\partial}{\partial x^{ik}}\right)$ denoted as a vector field and f_{i1} is assigned as coordinate function near point $p \in d\left(NC_{\boldsymbol{p}_{\{x,y,z\}}}\right)$ and then it yields $\sum_{i1<\dots<ik} \alpha_{i1} \dots \alpha_{ik}\, df_{i1} \wedge \dots \wedge df_{ik})$ [45]. Further, since statistical equations do not regulate the cellular processes, it requires defining how these interactions between the vector fields and every point on manifolds could be ruled by logical equations such as Boolean algebra at the time '*dt*' [46]. Hence, each of the mentioned contributing factors to cellular development $\{X_1 = \alpha(E)_k, X_2 = \beta(C)_l, X_3 = d\left(NC_{\boldsymbol{p}_{\{x,y,z\}}}\right)\}$ should be included in the *Boolean function* before implementing the above-mentioned equations (see **Figure 8.B**). Thus, the differential of a Boolean function is defined by $f(X_i \oplus dX_i) = (X_1 \oplus dX_1, \dots X_i \oplus dX_i)$, so the expression of $(X_i \oplus dX_i)$ implies {if X_i *value chnages then* $dX_i = 1$, otherwise the $dX_i = 0$}. Therefore, the *total differential function* is defined by $d_{X_i} f(X_i) = f(X_i) \oplus f(X_i \oplus dX_i)$, and the *total differential minimum* is denoted by $\min_{X_i} f(X_i) = f(X_i) \wedge f(X_i \oplus dX_i)$ *and total differential maximum* by $\max_{X_i} f(X_i) = f(X_i) \vee f(X_i \oplus dX_i)$.

Discussion

In this study, we tried to model the neurodevelopmental processes mathematically but, more importantly stressing the possibilities and the pitfalls while categorizing the neurodevelopment for simplicity into various approaches. We devised three approaches to understand from which aspect it should be addressed for testing the possibility of neurodevelopmental mathematical modelling. However, it is essential to first try to approximate the real dynamics underlying that specific process. It does not sound easy because, as we discussed in the **Figure 1**, it can be viewed and modelled in all the steps of neurodevelopment instead of just focusing on neuronal clustering during corticogenesis [5]. Comparatively, several theories do not provide a relevant computational formulation for neurodevelopmental processes. Most of the studies provide a mathematical framework for brain growth in the form of networks and wired nodes between different brain regions. They do not offer a specific parametrization for cellular characteristics or how the neurodevelopment process occurs based on mathematical and geometrical parameters similar to what we

proposed in this study. Instead, their findings are limited to the nodes and wiring changes, not the underlying mathematical/ geometrical mechanism contributing to neurodevelopment [3].

Further, the complexity of biology requires us to be cautious when we intend to do modelling. Therefore, to tackle this issue, we proposed at least two criteria that must be followed before thinking about mathematical modelling. It helps to consider them as they are two main elements, so-called naturally built-in, that mathematically should be regarded. They are briefly considered *holomorphic*, indicating continuity, complex-valued function, and group *homomorphism* that can transform into different structures. In the next step, we were interested in *cell division to neurodevelopment*, defined as the orientation and organization of cells as a function of cell division and polarity. As mentioned, this pattern and approach naturally occur in cells during division. The actin filaments under the cell membrane are the so-called "cell cortex" responsible for cell division and tissue morphogenesis [6,7]. So, we assumed that the *actin filaments* could be used to mathematically explore how to model the cell division and development. Still, it became complicated to generate the tissue model further based on this approach. However, this is a distinguishable finding when we model biological phenomena mathematically. We should not simply try to push fitting the mathematical equations into the underlying mechanisms existing in biological systems; instead, the critical point is discovering the appropriate approach and approximate mathematical modelling that includes the proper topological definition and providing proper, relevant algorithms for the underlying dynamics or mechanism.

Next, we tried the neural tube formation to neurodevelopment approach. It looks fascinating as the neuronal trajectory is projected all along the CNS longitudinally, so the neurons can be modelled accordingly, as we showed in this section and provided a simplified equation that geometrically tries to fit both the structural complexity and space formation.

Finally, we approached neural plate formation and *neurodevelopment. W*e could provide a model that fits most of the elements of the neurodevelopment, such as cellular characteristics, tissue growing in z axis according to a *numerical map* and a proposed equation that involves geometrical functions that behave like a fitting model to converge into two components by using a numerical solution, namely *Runge-Kutta method* [31]. The polynomial equation generated by the binominal formula connects to the numerical map (Pascal's triangles) and 'M' from **Figure 7.3**, which determines the individual cell growth and development in three axes that regulate whole tissue development.

This model meets many of the suggested requirements. However, as we don't know the exact numerical map, our understanding must be individualized for different tissue types, so we need to adjust the equations further. Further study is required to discover all components and complete this model that can generate the

whole brain. However, it was essential to develop a model that can be a platform for mathematical modelling of neurodevelopment. In the last part, we discuss and compare our proposed equation with the closest equivalent to our equation, the *Weierstrass Elliptic Function*. This equation uses lattice and *p-function* to generate the 3D objects in periodicity. This model has difficulty providing the proper parameters that can be adjusted for, e.g., the cell characteristics, controlling the continuous tissue growth (brain development) in z axis, or even mapping the growth. Therefore, in our experience, it would be almost impossible to provide a model with this equation without considering these issues. The last section of the result describes the mathematical concepts that reflect the process of neurodevelopment in terms of topological definition and change in the manifolds in interaction with the vector fields in the form of electrical and cellular Gibbs energy that all contribute to cell growth and tissue formation. The well-known diagram of Functors, Exterior Algebra, and Boolean functions was expressed and applied to present the process in mathematical terms and topological spaces. This information is helpful to clarify the details of neurodevelopment more topologically and better understand neurodevelopment in terms of mathematical terminology. It sheds light on the underlying mechanisms of biological and molecular processes regulated by sophisticated mathematical equations.

Conclusion

For the first time, we defined how to mathematically approach neurodevelopment regarding the underlying dynamics of neurodevelopment from different main aspects. We provided a unique model with details and a novel equation expected to fully model the whole brain tissue if the numerical map is discovered. Finally, we could define the process of neurodevelopment through a topological definition that includes the interaction of the manifolds with the vector fields in the form of electrical and cellular Gibbs energy. Finally, this approach is entirely novel based on how the natural contributing factors in terms of mathematical definition could explain the cellular growth and neurodevelopmental process.

Experimental procedures

In this study, different mathematical equations and algorithms were generated. In case needed, the written equations in the form of functions were implemented in MATLAB (R2021B) to generate the plots. The Latex of MATLAB was used for the shown formula. The Biorender (https://app.biorender.com/) was used to create the schematic illustrations.

Acknowledgements

This study was supported by Lundbeck Foundation, Frimurare Barnhusdirektionen, Magus Brevalls Stiftelse, Wilhelm och Martina Lundgrens Vetenskapsfond, Kronprinsessan Lovisas Förening För Barnasjukvård, Stiftelsen and Styrelsen för Stiftelsen Mary von Sydows, född Wijk Foundation.

Author Contributions

The Conceptualization, Methodology, Software, Formal Analysis, Writing – Original Draft were performed by A.H.R and MA. Resources, Writing – Review & Editing, Funding Acquisition were provided all by the following authors M.A., G.W. Writing – Review & Editing (constructive comments) are done by S.J and R.T.V. All authors reviewed the manuscript.

Declaration of interests

The authors declare no competing interests.

References

1 Noctor, S. C. *et al.* Dividing precursor cells of the embryonic cortical ventricular zone have morphological and molecular characteristics of radial glia. *Journal of Neuroscience* **22**, 3161-3173 (2002).
2 Stiles, J. & Jernigan, T. L. The basics of brain development. *Neuropsychology review* **20**, 327-348 (2010).
3 Akarca, D., Vértes, P. E., Bullmore, E. T. & Astle, D. E. A generative network model of neurodevelopment. *BioRxiv* (2020).
4 Rafati, A. H., Ardalan, M., Vontell, R. T., Mallard, C. & Wegener, G. Geometrical modelling of neuronal clustering and development. *Heliyon* **8**, e09871 (2022).
5 Nadarajah, B. & Parnavelas, J. G. Modes of neuronal migration in the developing cerebral cortex. *Nature Reviews Neuroscience* **3**, 423-432 (2002).
6 Chugh, P. & Paluch, E. K. The actin cortex at a glance. *Journal of cell science* **131**, jcs186254 (2018).
7 Pollard, T. D., Weihing, R. R. & Adelman, M. Actin and myosin and cell movemen. *CRC critical reviews in biochemistry* **2**, 1-65 (1974).
8 Yin, C., Jiang, H., Li, L., Lü, R. & Chen, S. Geometrical meaning of winding number and its characterization of topological phases in one-dimensional chiral non-Hermitian systems. *Physical Review A* **97**, 052115 (2018).
9 Weisstein, E. W. Kissing number. *https://mathworld. wolfram. com/* (2009).
10 Krier, N. in *Proc. Int. Conf. on Projective Planes, Washington State University, Pullman, Washington.* 157-163.
11 Gabcke, W. *Neue Herleitung und explizite Restabschätzung der Riemann-Siegel-Formel*, Georg-August-Universität Göttingen, (1979).
12 Humphries, S. P. Weak Cayley table groups. *Journal of Algebra* **216**, 135-158 (1999).
13 Pang, F. & Liu, M.-Q. Geometric isomorphism check for symmetric factorial designs. *Journal of Complexity* **27**, 441-448, doi:https://doi.org/10.1016/j.jco.2011.04.001 (2011).
14 Indritz, J. An inequality for Hermite polynomials. *Proceedings of the American Mathematical Society* **12**, 981-983 (1961).

15 Chen, B.-Y. Mean curvature and shape operator of isometric immersions in real-space-forms. *Glasgow Mathematical Journal* **38**, 87-97 (1996).
16 Margolis, B. *Differential Geometry: Part V Shape Operators*. (Open University Press, 1993).
17 Tseng, J.-L. & Lin, Y.-H. Low-resolution surface simplification using shape operators with large-scale surface analysis. *WIT Transactions on Information and Communication Technologies* **58**, 105-113 (2014).
18 Robinson, S. M. Normal maps induced by linear transformations. *Mathematics of Operations Research* **17**, 691-714 (1992).
19 REAL, A. Dynamical Systems Theory and Applications. (2017).
20 Snyder, G. & Song, Z. Koopman operator theory for nonlinear dynamic modeling using dynamic mode decomposition. *arXiv preprint arXiv:2110.08442* (2021).
21 Miller, J., Willard. Lie Theory and Separation of Variables. I: Parabolic Cylinder Coordinates. *SIAM Journal on Mathematical Analysis* **5**, 626-643 (1974).
22 Temme, N. M. Uniform asymptotic expansions of confluent hypergeometric functions. *IMA Journal of Applied Mathematics* **22**, 215-223 (1978).
23 Lee, T. C. & Vanstone, S. A. Subspaces and polynomial factorizations over finite fields. *Applicable Algebra in Engineering, Communication and Computing* **6**, 147-157 (1995).
24 Berger, M. *et al.* Affine spaces. *Problems in Geometry*, 11-17 (1984).
25 Pommersheim, J. E. Toric varieties, lattice points and Dedekind sums. *Mathematische Annalen* **295**, 1-24 (1993).
26 Liu, C.-S. & Kuo, C.-L. A multiple-scale Pascal polynomial triangle solving elliptic equations and inverse Cauchy problems. *Engineering Analysis with Boundary Elements* **62**, 35-43, doi:https://doi.org/10.1016/j.enganabound.2015.09.003 (2016).
27 Illarionov, A. A. e. Functional equations and Weierstrass sigma-functions. *Functional Analysis and Its Applications* **50**, 281-290 (2016).
28 Pastras, G. Four lectures on Weierstrass elliptic function and applications in classical and quantum mechanics. *arXiv preprint arXiv:1706.07371* (2017).
29 Salih, A. Classification of partial differential equations and canonical forms. *Lecture Notes, Department of Aerospace Engineering, Indian Institute of Space Science and Technology, Thiruvananthapuram* (2014).
30 Demengel, F. *Functional spaces for the theory of elliptic partial differential equations*. (Springer, 2012).
31 Verner, J. H. Numerically optimal Runge–Kutta pairs with interpolants. *Numerical Algorithms* **53**, 383-396 (2010).
32 Ostermann, A. & Roche, M. Runge-Kutta methods for partial differential equations and fractional orders of convergence. *Mathematics of computation* **59**, 403-420 (1992).
33 Ortiz-Bobadilla, L., Rosales-González, E. & Voronin, S. Analytic Classification of Foliations Induced by Germs of Holomorphic Vector Fields in (ℂ n, 0) (C^n,0) with Non-isolated Singularities. *Journal of Dynamical and Control Systems* **25**, 491-516 (2019).
34 Aduddell, R. *et al.* A compositional account of motifs, mechanisms, and dynamics in biochemical regulatory networks. *arXiv preprint arXiv:2301.01445* (2023).
35 Roman, S. *An introduction to the language of category theory*. Vol. 6 (Springer, 2017).
36 Rong, W. The countabilities of soft topological spaces. *International Journal of Mathematical and Computational Sciences* **6**, 952-955 (2012).
37 Ganster, M. A note on strongly Lindelöf spaces. *Soochow J. Math* **15**, 99-104 (1989).
38 Xuan, W.-F. & Song, Y.-K. More on cellular-Lindelöf spaces. *Topology and its Applications* **266**, 106861 (2019).
39 Vogt, D. in *North-Holland Mathematics Studies* Vol. 27 167-187 (Elsevier, 1977).
40 El Baz, M. & Hassouni, Y. Deformed exterior algebra, quons and their coherent states. *International Journal of Modern Physics A* **18**, 3015-3040 (2003).

41 Alberty, R. A. Use of Legendre transforms in chemical thermodynamics (IUPAC Technical Report). *Pure and Applied Chemistry* **73**, 1349-1380 (2001).
42 Lamorgese, A., Mauri, R. & Sagis, L. Modeling soft interface dominated systems: A comparison of phase field and Gibbs dividing surface models. *Physics Reports* **675**, 1-54 (2017).
43 Aledo, J. C. Metabolic pathways: does the actual Gibbs free-energy change affect the flux rate? *Biochemistry and molecular biology education* **29**, 142-143 (2001).
44 Katz, V. J. Differential forms-Cartan to de Rham. *Archive for history of exact sciences*, 321-336 (1985).
45 Gross, G. & Meinrenken, E. *Manifolds, vector fields, and differential forms: an introduction to differential geometry*. (Springer Nature, 2023).
46 Steinbach, B. & Posthoff, C. in *Logic Functions and Equations: Fundamentals and Applications using the XBOOLE-Monitor* 225-295 (Springer, 2021).

Figure Legend:

Figure 1. The schematic illustration of three Steps of neurodevelopment. A. Cell division where the pack of cells resemble "kissing number" B. Neural plate formation, C. Neural tube formation.

Figure 2. A. Cell division polarization and the simple 3D cell organization. B. The assumed cell-shell complex fibres called "cellular cortex" correspond to the mathematical model for simplicity of generating the following structures.

Figure 3. A. The shapes of cells during division and polarization when using the complex fibres are called the complex values of "Wi. B. The radiated lines highlight how the curves are distributed in the space around the centre of the dividing cell.

Figure 4. A. Three curves C, S, S´. The S and S´ cross, the midline curve C, symmetrically looks like the CNS trajectories crossing all along, designed similar to "Möbius plane" B. The plot is the mathematical equivalence of the speculation in A, as it shows here, it is a symmetrical distribution of two curves around the midline curve. C. Two schematic illustrations are representative of CNS.

Figure 5. A. It shows a neuron with its long axon. B, C. They demonstrate two different equations with similar shapes that can reflect single-unit neurons. It is assumed that theoretically, using this unit would help the mathematical neurodevelopment model like figure 4. C.

Figure 6.A. The left object shows a shape change in a spheroid cell, while the right shows two blue spheres reflecting the shape operator ($S_p(v)$=$-\nabla_v N$) with unit normal vectors (N) on the brown curves that show how the curves are moving in every direction during the cellular shape change. B. The mapping and transformation are illustrated clearly by an example of how transformation might occur using (f**:** x → x´). C. An example of a so-called parabolic cylinder coordinate shows the spatial orientation and organization of cylinders in relation to manifolds. D. It shows how the cells migrate

and organize through the layers from bottom to top, like in a neural plate. The last item shows the bijective function (***f*****:** X → Y), an isomorphism, and its map is an example of mathematical modelling of tissue growth.

Figure 7.1. A. Schematic illustration shows how the neuronal progenitors change shape and direction during neurodevelopment. This illustration is related to our previous study [4], in which we designed how cell shape, direction, and electrical activity are defined as independent elements for neurodevelopment. The 3D position of cells in beginning= $\{\hat{\imath}, \hat{\jmath}, \hat{k}\}$, the G function and its parameters as The change in position of cells = $\{dp_1, dp_2, dp_3\}$, Shapes= Sphere, ellipsoid, pyramidal approximation, other convex bodies, Electrical activity= Excitatory $\{+\}$, Inhibitory $\{-\}$, Excitatory/Inhibitory $\{\pm\}$, X (dp_1, s, e_1), Y (dp_2, s, e_2), Z (dp_3, s, e_3). B. It represents the "*Linear subspace"* in a finite field indicated by circles and connecting linear. The Pascal's triangle is located above it. The schematic illustration of coloured cells in the x-y plane is analogous to *Linear subspace"* in a finite field. The neuronal growth and organization in the z-axis are shown.

Figure 7.2. A. The schematic illustration shows the steps that cells grow vertically using a "*linear subspace*", as explained in the Figure.7.1, then we have shown the vertical "black curves", which are indeed '*Bezier curve*' generated by using equation.1 and grows vertically/obliquely according to the *Pascal triangle*, for example, the $t_3 = x^3 + 3x^2y + 3xy^2 + y^3$ is generated by the 3rd line of the Pascal triangle and is along the orange circles while connecting the "3" points; they are curvilinear lines that determine the whole shape of tissue in that certain section. However, the height and growth direction of each cell are more sophisticated and determined by curves that are a function of "W" calculated from equation.1 and "M" (see text), respectively. The circles represent different cell types with their specific properties, summarized in "M". B. It shows the next steps of the growing that there is a "*yellow line."* $t_5 = x^5 + 5x^4y + \mathbf{10\,x^3y^2} + 10x^2y^3 + 5xy^3 + y^5$ through the yellow circles generated based on the "*specific row*" in the "*Pascals triangle*". As shown, the black circle could be a "*singularity"*, so it differs from other circles therefore that one can be removed $\mathbf{10\,x^3y^2}$ (see text) and the rest of the equation will appear differently when plotted. This singularity can be equivalent to a specific cell type or extracellular matrix. C. It shows two consecutive limited '*Pascals triangle*'; the binominal coefficient yields it and generates the equations (t_1:t_n) accordingly. D. It depicts a circle and an ellipsoid; they have two curves generated by two vectors using equation.1, '*Bezier Curve*'.

Figure 7.3. The schematic illustration of the steps of the whole mathematical process of our proposed model. It starts with the equation, ends in developing cells and repeats continuously until complete implementing according to, as an example, *the Pascals triangle*.

Figure 8. The summary of the equation involved in NC growth and development. A. It demonstrates the diagram of the Functors and the *natural transformation* denoted by Φ and how commutes: Cf o Φ(M1) = Φ(M2) o Ef. B. It demonstrates an example of a differential Boolean function in the form of graph G (Xi, dXi) and shows how dXi changes are dependent on Xi changes. The Xi represents the factors $X_1 = \alpha(E)_k$, $X_2 = \beta(C)_l$, $X_3 = d\left(NC_{\boldsymbol{p}_{\{x,y,z\}}}\right)$ that determine how the dXi changes, for example, $(\overline{X1}, \overline{X2}, \overline{X3})$=[0,0,0] can change in value as follows $(X1, \overline{X2}, \overline{X3})$=[1,0,0]. The G1, G2, and G3 are shown in red with distinguished pathways accordingly. C. It shows the relation between the factors involved in cell growth and development for every point of *p* of manifold, NC(M1). It needs to implement the interaction of vector fields on NC(M1) such that $\oint(\alpha \wedge \beta)\left(X_{S(1)}, X_{S(i)\ldots}, X_{S(k)}\right) dt$, it integrates each time (dt) that receives the G=1 in which the G is a function of Xi changes in the form of inputs. D. The whole process of NC(M1)→NC(M2) is shown here. The vector fields of V_C and V_E at point $P_{\{x, y, z\}}$ are shown. The Cf o Φ(M1) = Φ(M2) o Ef represents the interaction of functors and vector fields, and natural transformation is reflected as the schematic illustration in the form of interaction between NC and vector fields.

Figures

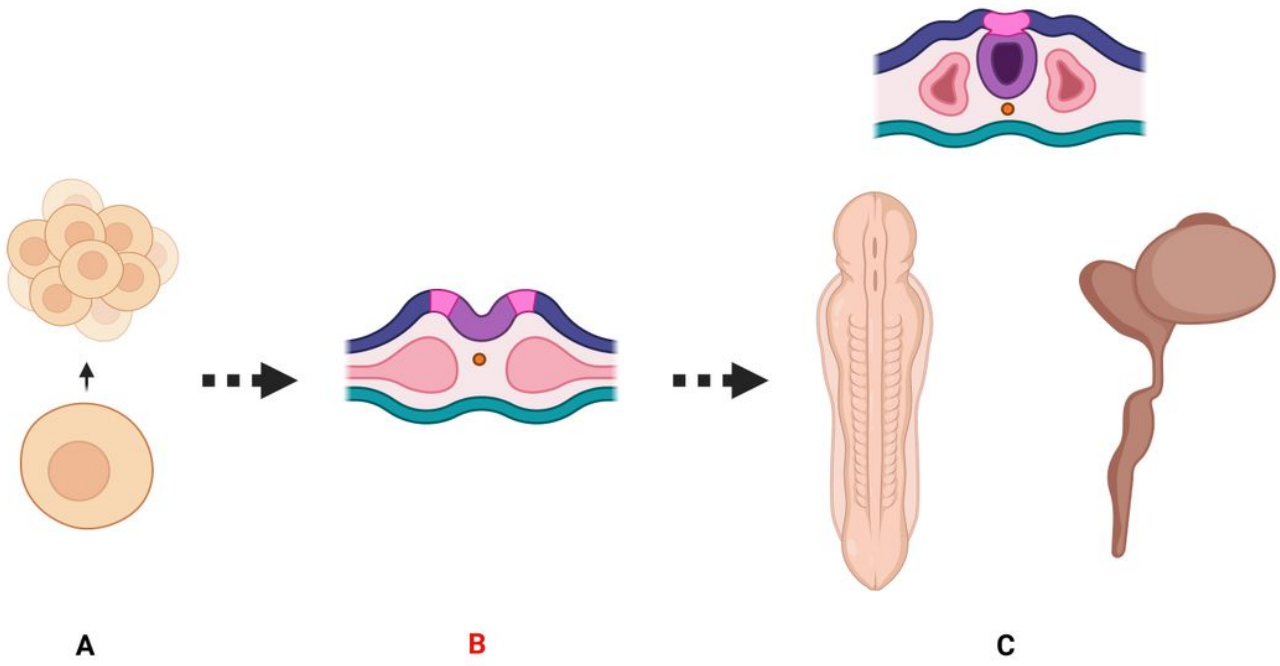

Figure 1

The schematic illustration of three Steps of neurodevelopment. A. Cell division where the pack of cells resemble “kissing number” B. Neural plate formation, C. Neural tube formation.

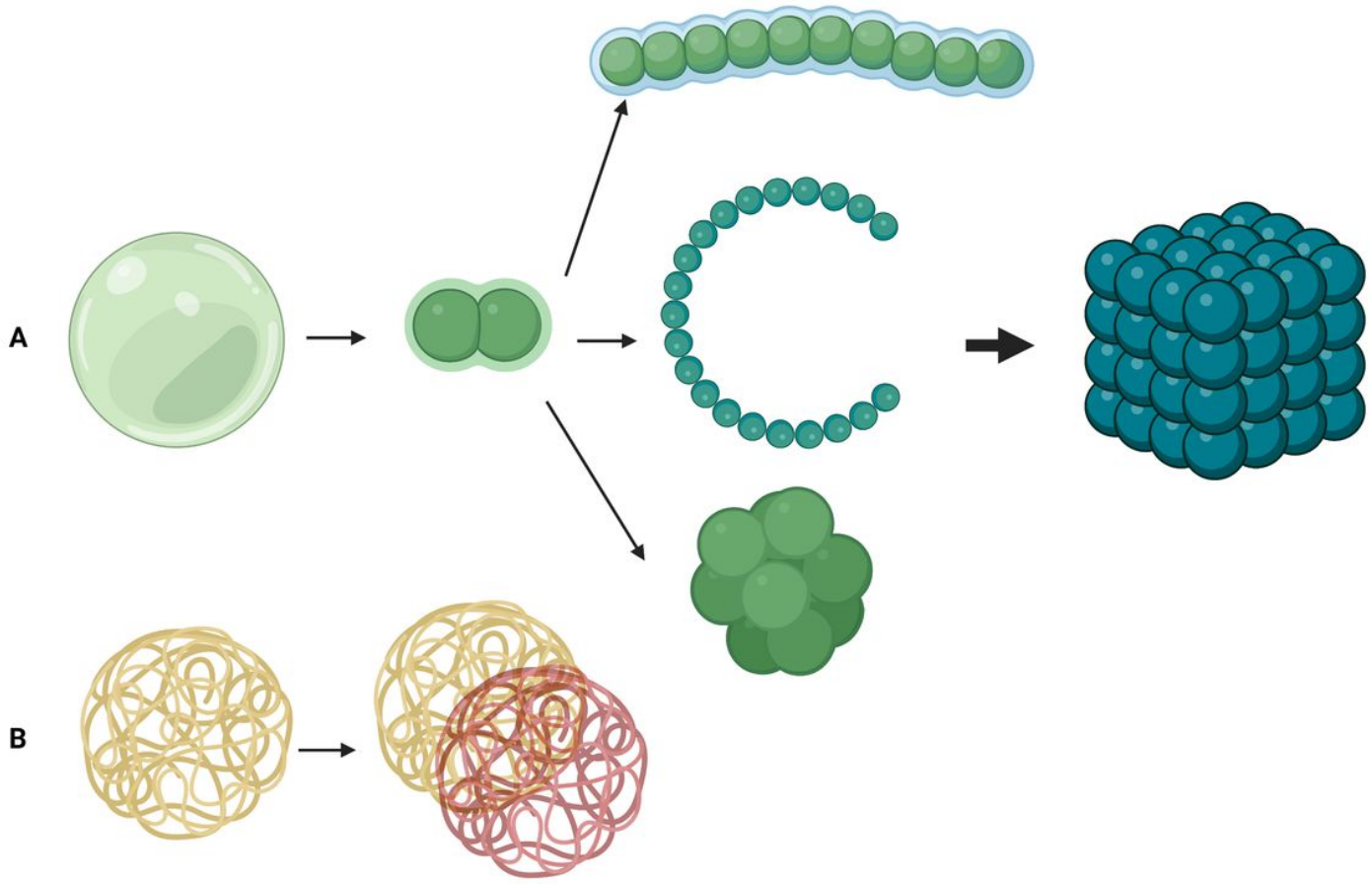

Figure 2

A. Cell division polarization and the simple 3D cell organization. B. The assumed cell-shell complex fibres called “cellular cortex” correspond to the mathematical model for simplicity of generating the following structures.

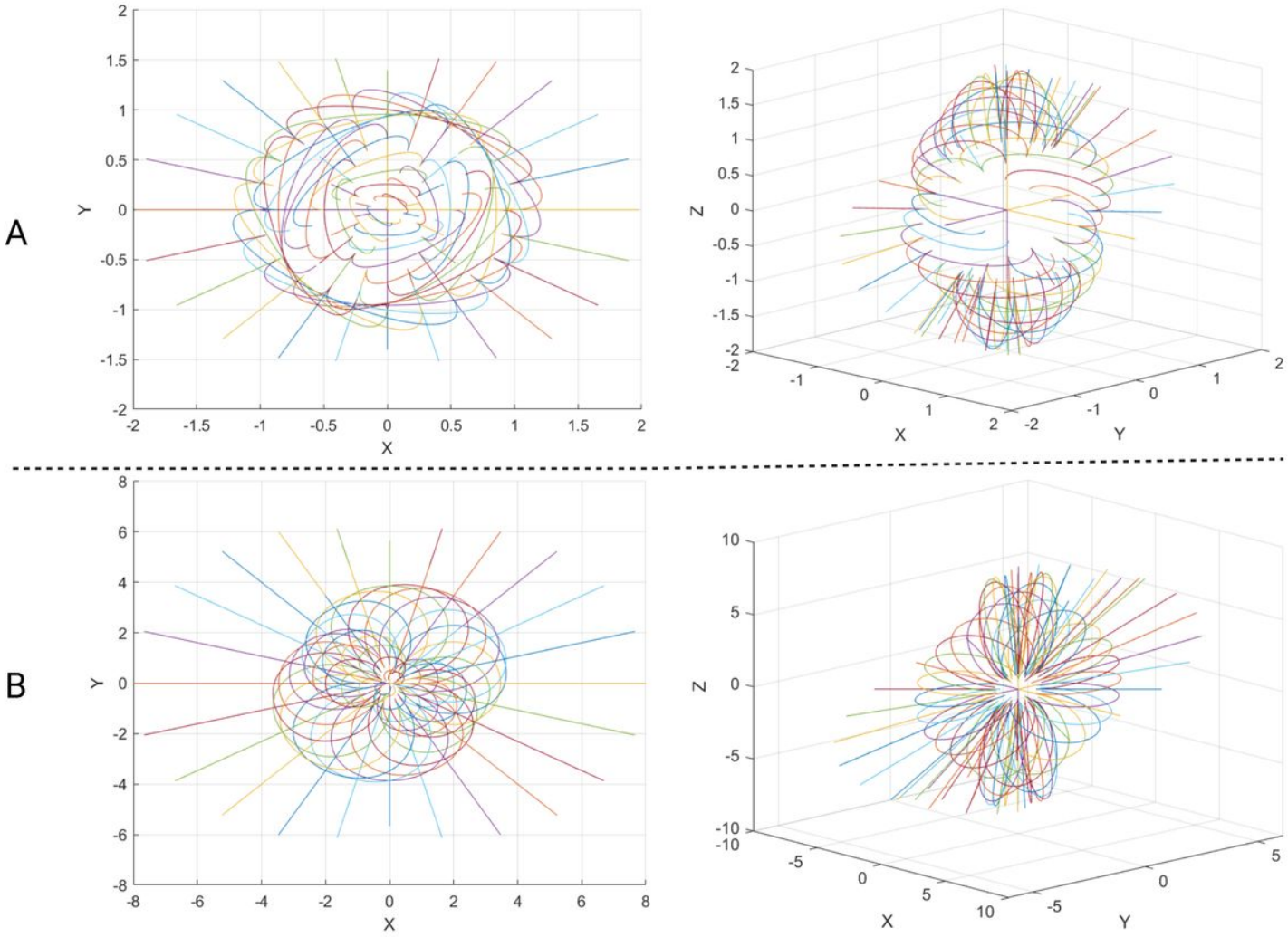

Figure 3

A. The shapes of cells during division and polarization when using the complex fibres are called the complex values of “Wi. B. The radiated lines highlight how the curves are distributed in the space around the centre of the dividing cell.

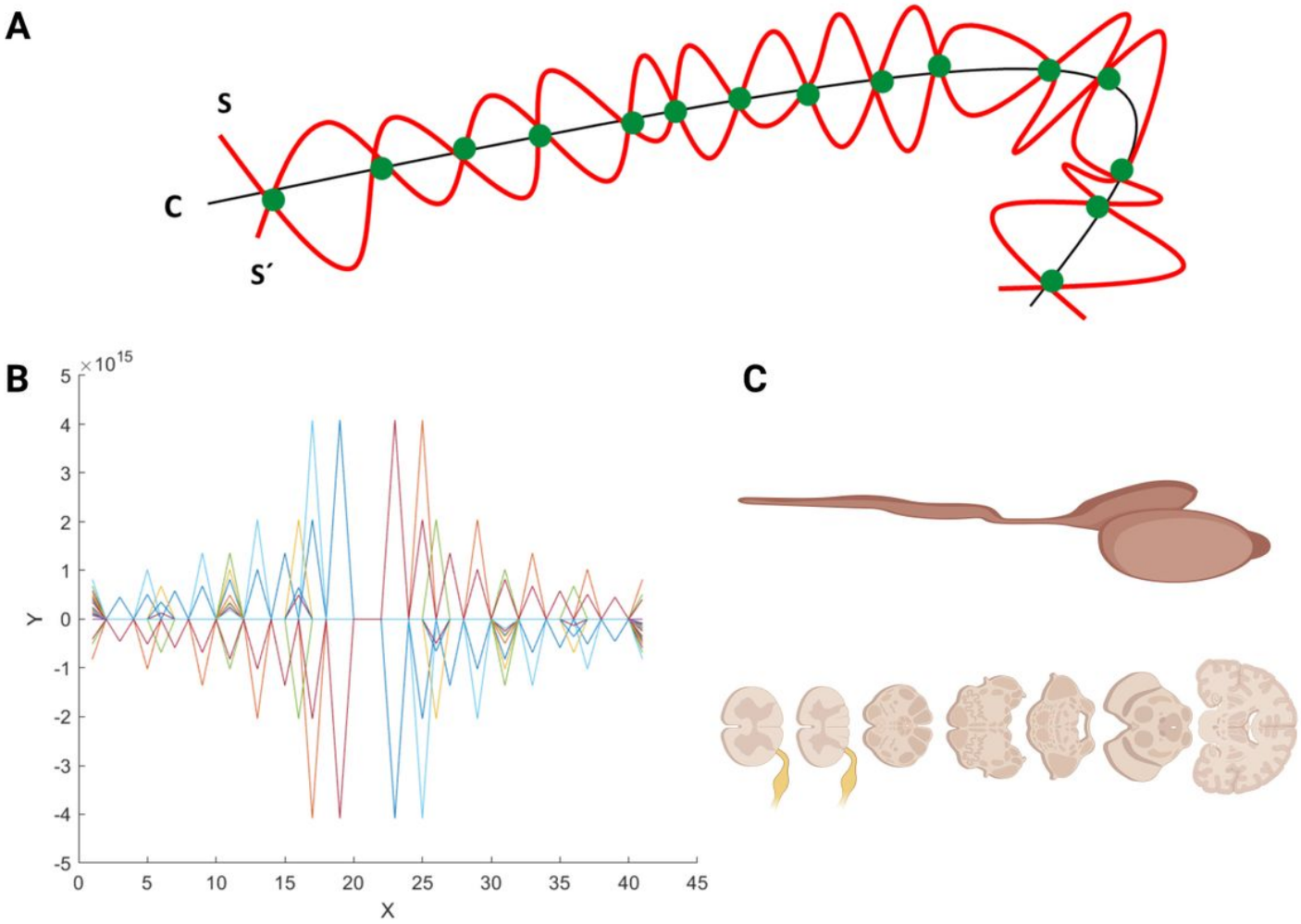

Figure 4

A. Three curves C, S, S´. The S and S´ cross, the midline curve C, symmetrically looks like the CNS trajectories crossing all along, designed similar to “Möbius plane” B. The plot is the mathematical equivalence of the speculation in A, as it shows here, it is a symmetrical distribution of two curves around the midline curve. C. Two schematic illustrations are representative of CNS.

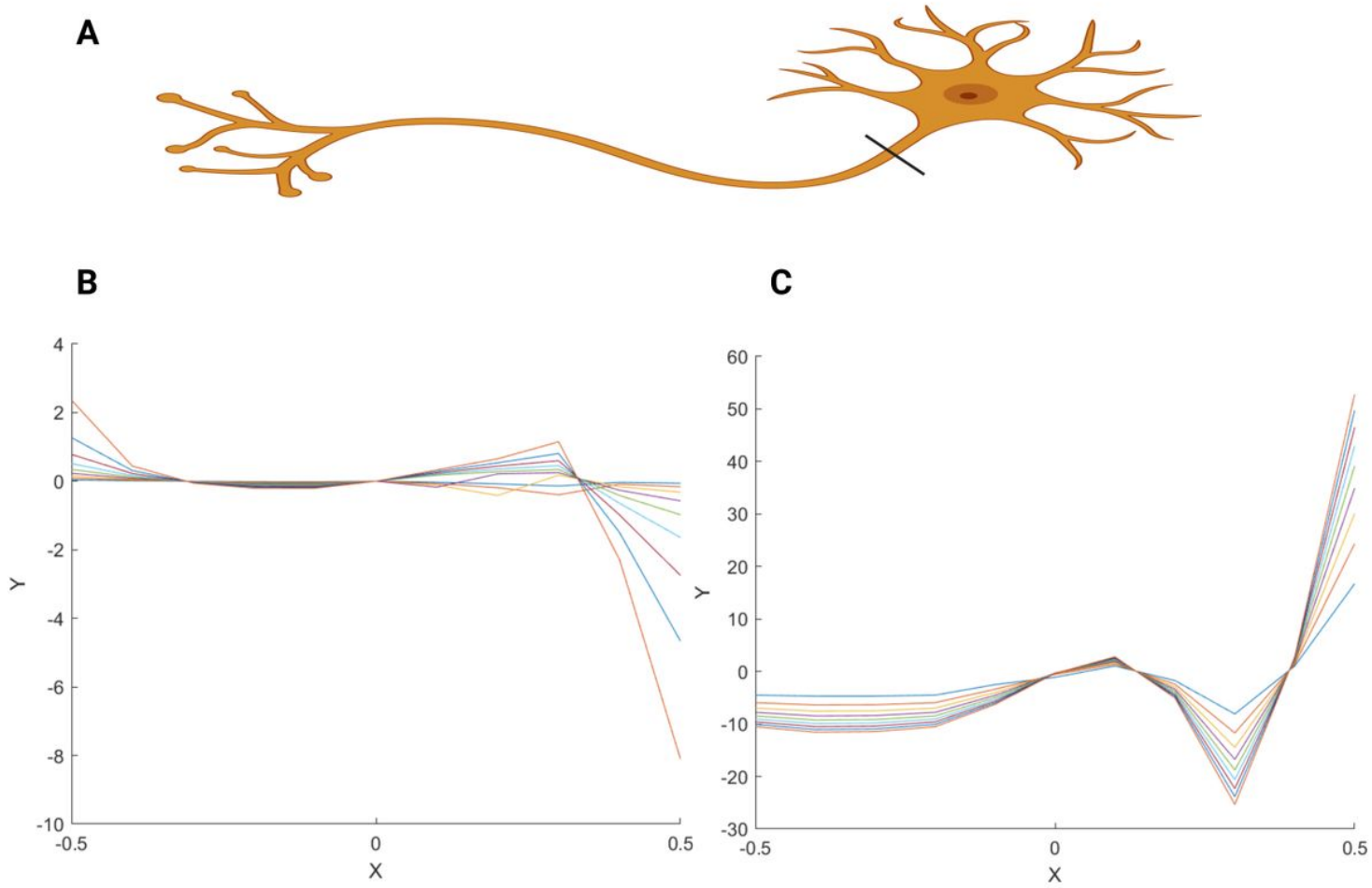

Figure 5

A. It shows a neuron with its long axon. B, C. They demonstrate two different equations with similar shapes that can reflect single-unit neurons. It is assumed that theoretically, using this unit would help the mathematical neurodevelopment model like figure 4. C.

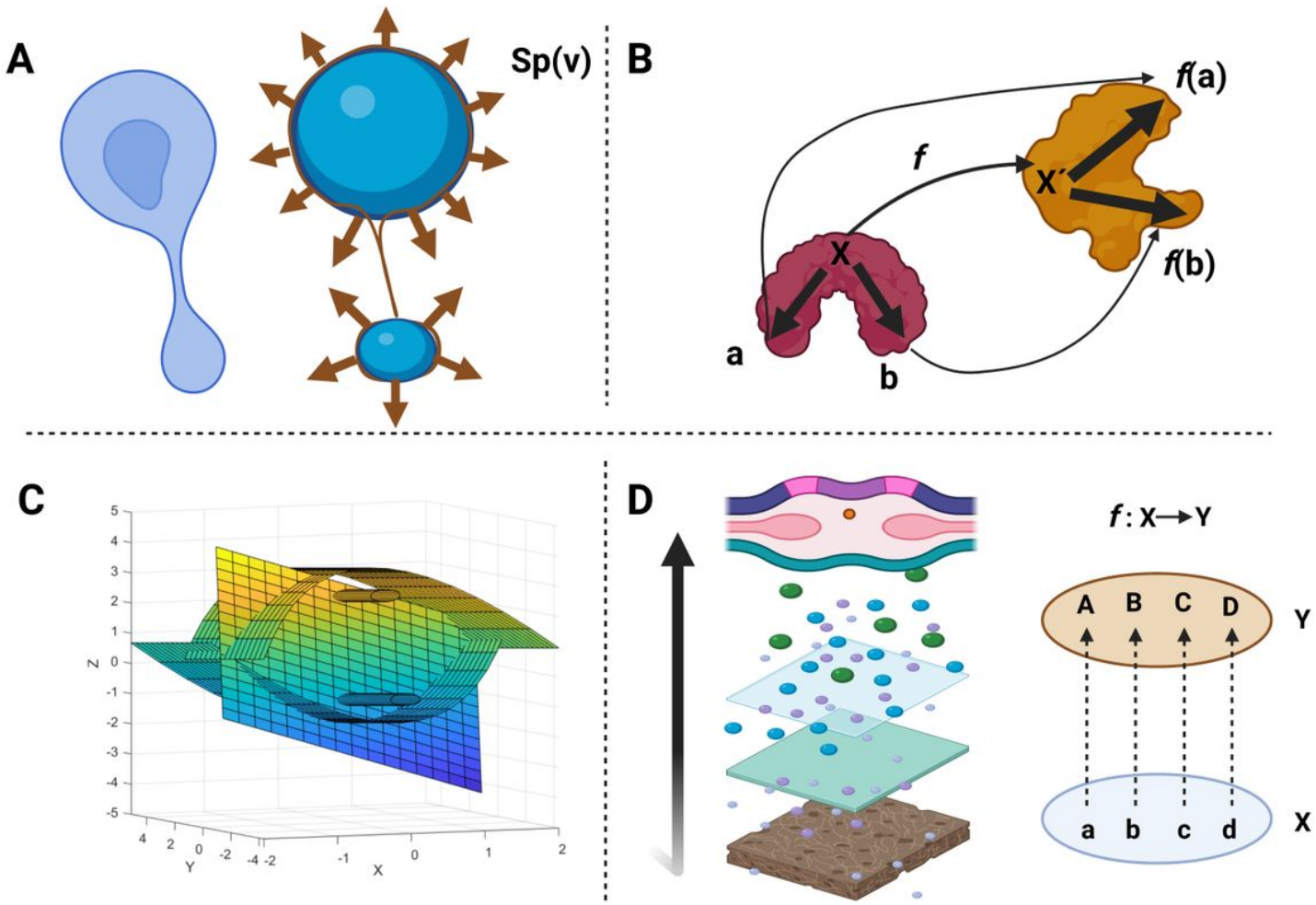

Figure 6.A. The left object shows a shape change in a spheroid cell, while the right shows two blue spheres reflecting the shape operator ($S_p(v) \mapsto -\nabla_v N$) with unit normal vectors (N) on the brown curves that show how the curves are moving in every direction during the cellular shape change. B. The mapping and transformation are illustrated clearly by an example of how transformation might occur using (f: x → x'). C. An example of a so-called parabolic cylinder coordinate shows the spatial orientation and organization of cylinders in relation to manifolds. D. It shows how the cells migrate and organize through the layers from bottom to top, like in a neural plate. The last item shows the bijective function (*f*: X → Y), an isomorphism, and its map is an example of mathematical modelling of tissue growth.

Figure 6

See image above for figure legend

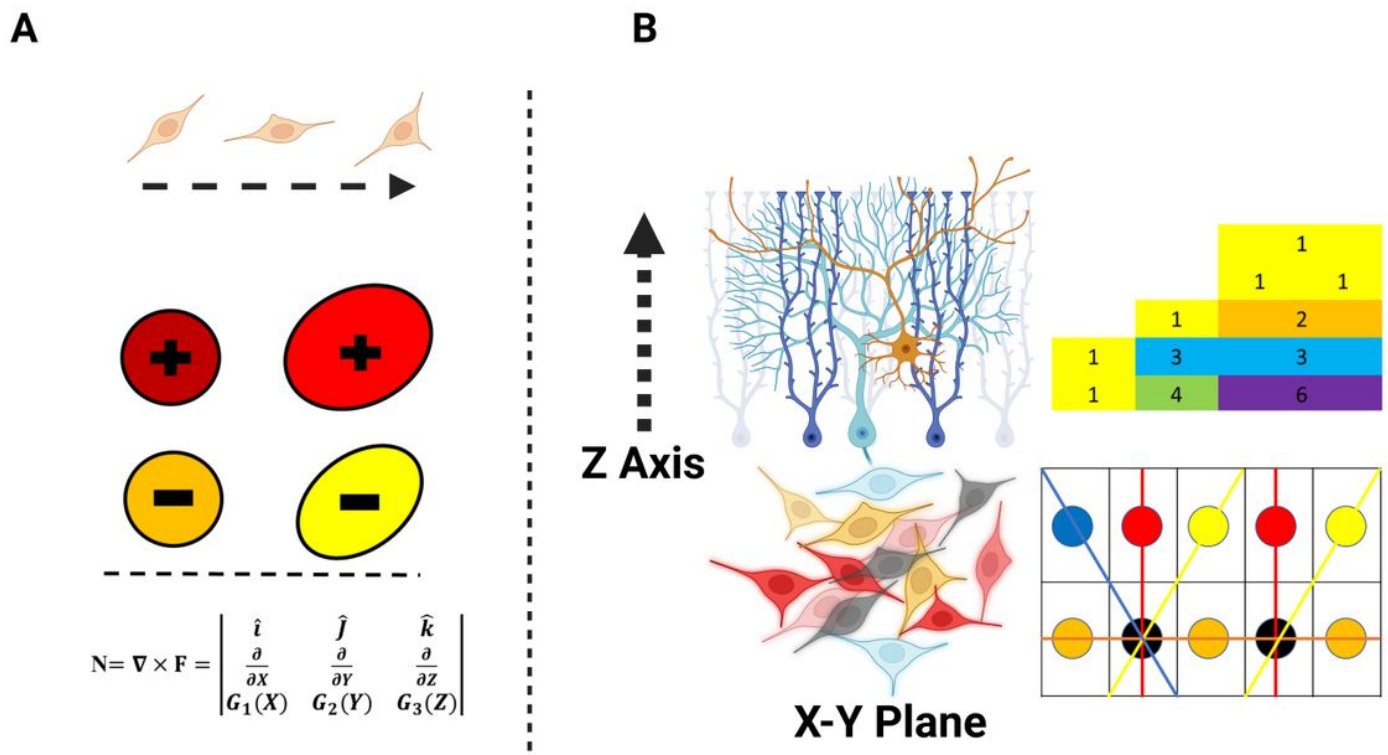

Figure 7.1. A. Schematic illustration shows how the neuronal progenitors change shape and direction during neurodevelopment. This illustration is related to our previous study [4], in which we designed how cell shape, direction, and electrical activity are defined as independent elements for neurodevelopment. The 3D position of cells in beginning= $\{\hat{\imath}, \hat{\jmath}, \hat{k}\}$, the G function and its parameters as The change in position of cells = $\{dp_1, dp_2, dp_3\}$, Shapes= Sphere, ellipsoid, pyramidal approximation, other convex bodies, Electrical activity= Excitatory $\{+\}$, Inhibitory $\{-\}$, Excitatory/Inhibitory $\{\pm\}$, X (dp_1, s, e_1), Y (dp_2, s, e_2), Z (dp_3, s, e_3). B. It represents the "*Linear subspace*" in a finite field indicated by circles and connecting linear. The Pascal's triangle is located above it. The schematic illustration of coloured cells in the x-y plane is analogous to *Linear subspace*" in a finite field. The neuronal growth and organization in the z-axis are shown.

Figure 7

See image above for figure legend

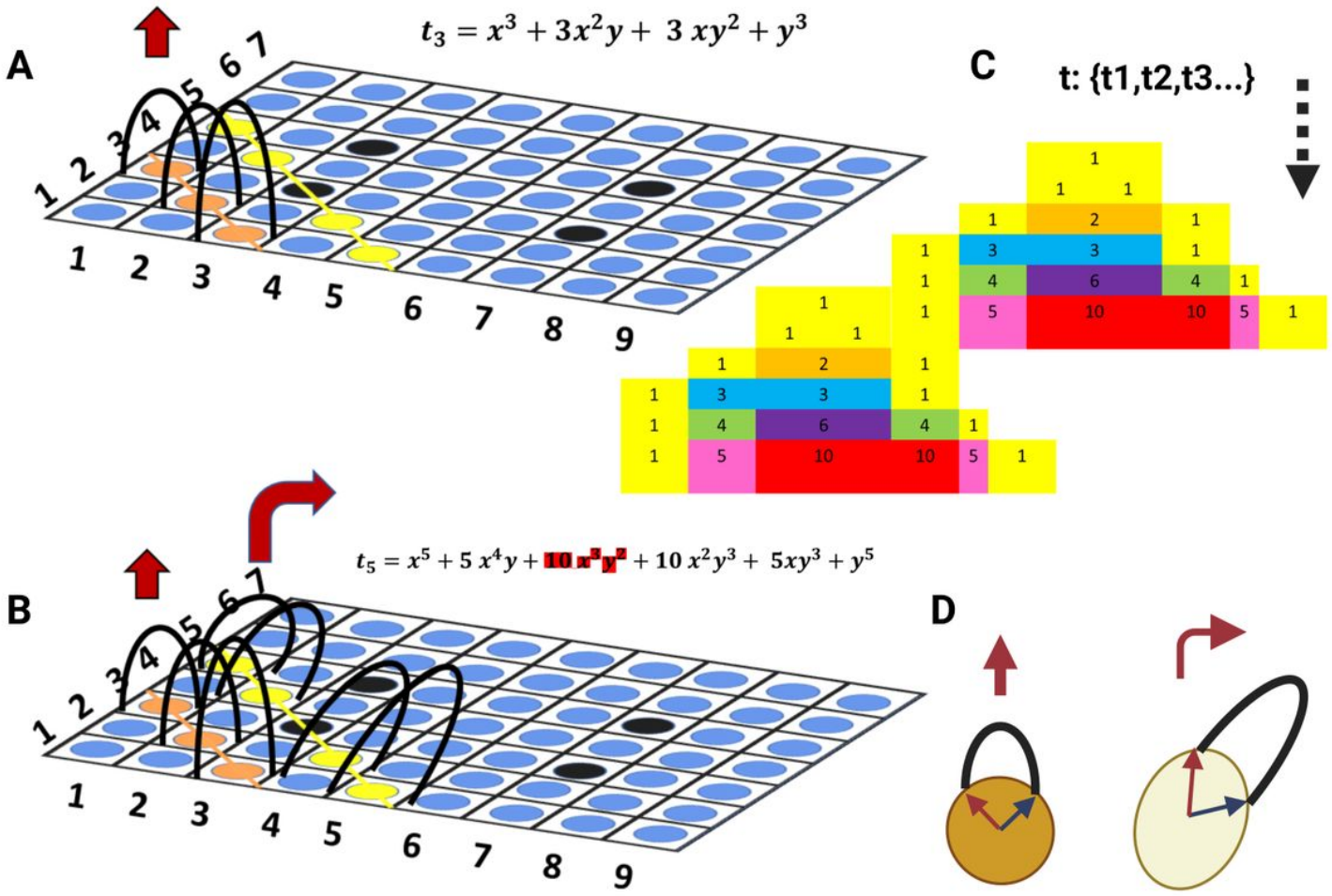

Figure 7.2. A. The schematic illustration shows the steps that cells grow vertically using a *"linear subspace"*, as explained in the Figure.7.1, then we have shown the vertical "black curves", which are indeed '*Bezier curve*' generated by using equation.1 and grows vertically/obliquely according to the *Pascal triangle*, for example, the $t_3 = x^3 + 3x^2y + 3xy^2 + y^3$ is generated by the 3rd line of the Pascal triangle and is along the orange circles while connecting the "3" points; they are curvilinear lines that determine the whole shape of tissue in that certain section. However, the height and growth direction of each cell are more sophisticated and determined by curves that are a function of "W" calculated from equation.1 and "M" (see text), respectively. The circles represent different cell types with their specific properties, summarized in "M". B. It shows the next steps of the growing that there is a *"yellow line."* $t_5 = x^5 + 5x^4y + \mathbf{10x^3y^2} + 10x^2y^3 + 5xy^3 + y^5$ through the yellow circles generated based on the "*specific row*" in the "*Pascals triangle*". As shown, the black circle could be a "*singularity*", so it differs from other circles therefore that one can be removed $\mathbf{10x^3y^2}$ (see text) and the rest of the equation will appear differently when plotted. This singularity can be equivalent to a specific cell type or extracellular matrix. C. It shows two consecutive limited '*Pascals triangle*'; the binominal coefficient yields it and generates the equations (t_1:t_3) accordingly. D. It depicts a circle and an ellipsoid; they have two curves generated by two vectors using equation.1, '*Bezier Curve*'.

Figure 8

See image above for figure legend

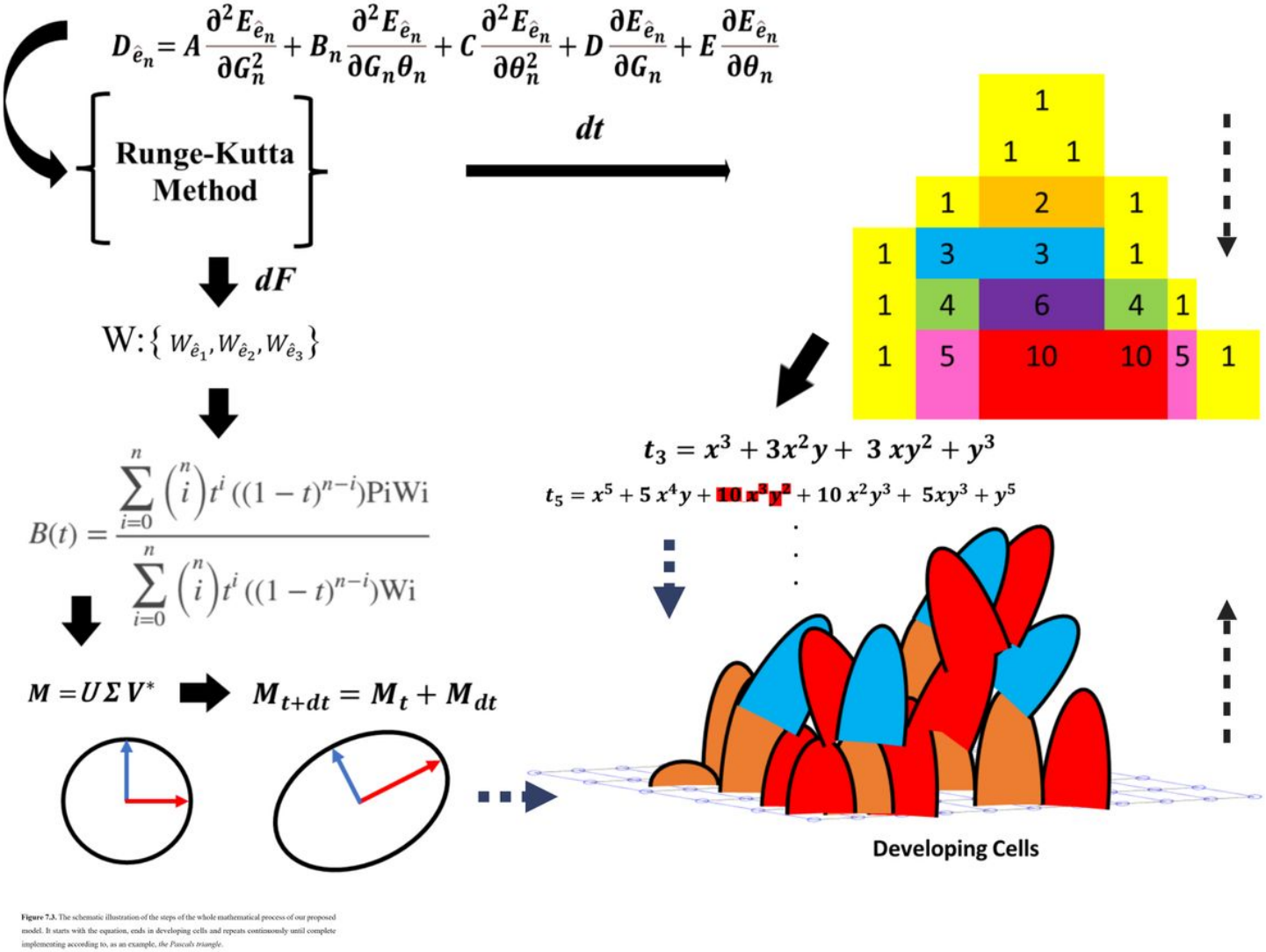

Figure 7.3. The schematic illustration of the steps of the whole mathematical process of our proposed model. It starts with the equation, ends in developing cells and repeats continuously until complete implementing according to, as an example, *the Pascal's triangle*.

Figure 9

See image above for figure legend

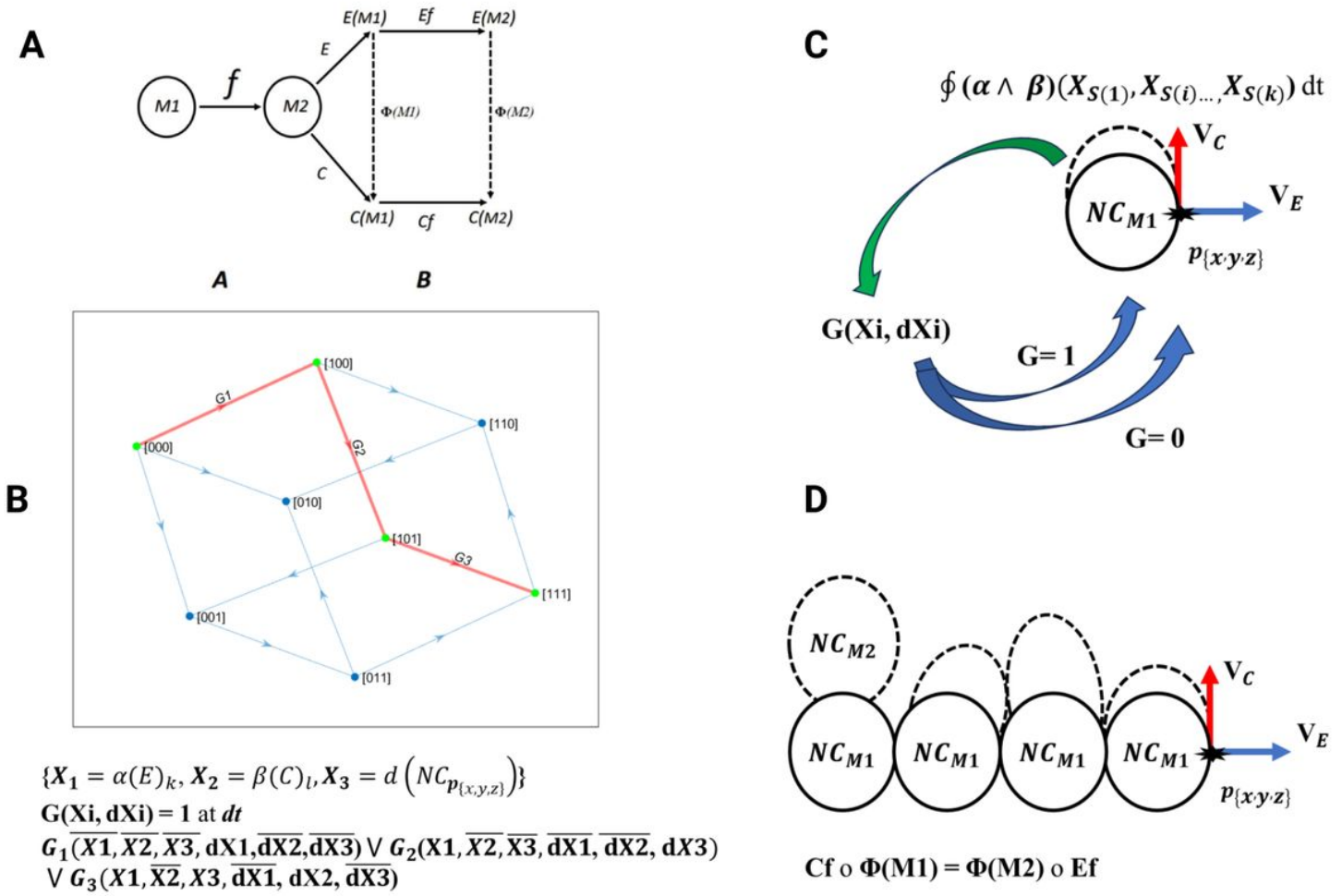

Figure 8. The summary of the equation involved in NC growth and development. A. It demonstrates the diagram of the Functors and the *natural transformation* denoted by Φ and how commutes: Cf o Φ(M1) = Φ(M2) o Ef. B. It demonstrates an example of a differential Boolean function in the form of graph G (Xi, dXi) and shows how dXi changes are dependent on Xi changes. The Xi represents the factors $X_1 = \alpha(E)_k$, $X_2 = \beta(C)_l$, $X_3 = d\left(NC_{p_{\{x,y,z\}}}\right)$ that determine how the dXi changes, for example, $(\overline{X1}, \overline{X2}, \overline{X3}) = \{0,0,0\}$ can change in value as follows $(X1, \overline{X2}, \overline{X3}) = \{1,0,0\}$. The G1, G2, and G3 are shown in red with distinguished pathways accordingly. C. It shows the relation between the factors involved in cell growth and development for every point of p of manifold, NC(M1). It needs to implement the interaction of vector fields on NC(M1) such that $\oint(\alpha \wedge \beta)(X_{S(1)}, X_{S(i)\ldots}, X_{S(k)})\,dt$, it integrates each time (dt) that receives the G=1 in which the G is a function of Xi changes in the form of inputs. D. The whole process of NC(M1)→NC(M2) is shown here. The vector fields of V_C and V_E at point $P_{\{x, y, z\}}$ are shown. The Cf o Φ(M1) = Φ(M2) o Ef represents the interaction of functors and vector fields, and natural transformation is reflected as the schematic illustration in the form of interaction between NC and vector fields.

Figure 10

See image above for figure legend

Supplementary Files

This is a list of supplementary files associated with this preprint. Click to download.

- GraphicalAbstract.tiff